# Innovative use of industrially produced steel slag powders in asphalt mixture to replace mineral fillers

Zongwu Chen[1, 2, 3, 4, 5], Zhen Leng[1*], Yuyong Jiao[5], Fang Xu[5], Juntao Lin[5], Haopeng Wang [6], Jun Cai[7], Linlu Zhu[5], Yunlong Zhang[5], Namin Feng[5], Yidan Dong[5], Yang Zhang[5]

*[1] Department of Civil and Environmental Engineering, The Hong Kong Polytechnic University, Hong Kong, China*

*[2] Key Laboratory of Road Structure and Material of Ministry of Transport (Changsha), Changsha University of Science & Technology, Changsha, China*

*[3] State Key Laboratory of Green Building Materials, China Building Materials Academy, Beijing 100024, China*

*[4] State Key Laboratory of Subtropical Building Science, South China University of Technology, Guangzhou 510640, China*

*[5] Faculty of Engineering, China University of Geosciences (Wuhan), Wuhan, China*

*[6] Nottingham Transportation Engineering Centre, University of Nottingham, Nottingham, UK*

*[7] Key Laboratory of Special Environment Road Engineering of Hunan Province, Changsha University of Science & Technology, Changsha, China*

**Abstract:** Using steel slag to partially replace the natural aggregate in asphalt mixture to produce high-performance asphalt mixture has gained significant interest in recent years as a value-added option to recycle steel slag. However, the poor homogeneity of the properties of steel slag aggregates remains a concern for this recycling approach. In this study, an innovative method of using steel slag powder (SSP) to replace the mineral filler in asphalt mixture was proposed to address this concern. Five fillers, including four SSP fillers, obtained by grinding different steel slag aggregates with an industrialized production line, and one conventional limestone powder (LP) filler, were evaluated. The chemical compositions and micro-morphologies of the SSPs were first characterized to evaluate the material homogeneity and gain insights into the advantages of using SSPs as fillers. Then, asphalt mixtures with different fillers were designed and produced, and their moisture stability, rutting resistance, and low-temperature crack resistance, were characterized. It was found that the industrially produced SSPs possess homogeneous properties, and improved the compatibility between filler particles and asphalt binder, thus enhancing the bonding between asphalt mastic and aggregates. Besides, the asphalt mixtures with SSP fillers showed better

[*] Corresponding author.

E-mail address: zhen.leng@polyu.edu.hk (Z. Leng).

resistance to moisture damage, permanent deformation and low-temperature crack, than the mixture with the LP filler. Therefore, it was concluded that using SSPs as a replacement of mineral fillers in asphalt mixture provides a reliable and value-added solution to recycle steel slag.

**Keywords:** Steel slag powder; material property; filler; asphalt mixture; engineering performance

## 1. Introduction

Asphaltic materials have been widely used as road surfacing materials worldwide (Chang et al., 2020; Wang et al., 2020). For example, more than 90% of high-grade pavement in China are paved with asphaltic surfaces. This is mainly because asphalt pavement possesses excellent service performance, such as driving comfort, low noise, good skid resistance and easy maintenance. According to the official statistics of the Ministry of Transport (MOT) of the People's Republic of China, the total mileage of traffic roads has increased about 10.7% during the past five years in China (MOT, 2021), which causes significantly increased consumption of natural resources, such as aggregate and asphalt binder. Meanwhile, China, just like many other countries, is also facing the high demand of pavement maintenance. Therefore, developing greener and more sustainable materials for pavement construction and maintenance has become an urgent task. Correspondingly, recycling of appropriate solid wastes in asphalt pavement has become a hot topic, which is a very promising way to reduce the exploitation of natural resources. For example, steel slag (Ahmedzade and Sengoz, 2009; Chen et al., 2018; Chen et al., 2015; Chen et al., 2016a; Chen et al., 2016b; Huang et al., 2007; Shen et al., 2009; Xie et al., 2012; Xue et al., 2006), reclaimed asphalt pavement (RAP) (Leng et al., 2018b; Xiao et al., 2007; Xiao et al., 2009), waste plastic (Huang et al., 2007) and waste rubber (Huang et al., 2007; Xiao et al., 2009) have been used to partially replace natural aggregate in asphalt mixture; steel slag (Li et al., 2017a; Li et al., 2017b) and flue gas desulfurization ash (Chen et al., 2014a; Chen et al., 2014b) have been applied to replace asphalt filler; and waste plastic (Huang et al., 2007; Leng et al., 2018a; Leng et al., 2018b) and waste rubber (Huang et al., 2007; Xiao et al., 2007) have been recycled as asphalt binder modifiers.

Steel slag, generated during steelmaking, is a typical solid waste, which accounts for about 13% of raw steel output (Shen et al., 2009). The total utilization rate of steel slag is less than 30% in China, which is quite low considering the large quantity. Using steel slags as raw materials in asphalt mixture has been proved an effective recycling method (Ahmedzade and Sengoz, 2009; Chen et al., 2018; Chen et al., 2015; Chen et al., 2016a; Chen et al., 2014b; Chen et al., 2014c;

Pasetto et al., 2017; Shen et al., 2009; Wu et al., 2007; Xie et al., 2013; Xie et al., 2012; Xue et al., 2006). Many previous studies reported that the asphalt mixtures with steel slag aggregate (SSA) presented excellent skid resistance, high-temperature stability and fatigue durability (Ahmedzade and Sengoz, 2009; Chen et al., 2014b; Shen et al., 2009; Wu et al., 2007; Xie et al., 2013; Xue et al., 2006). However, different findings have been reported regarding their moisture stability (Chen et al., 2020; Chen et al., 2016a; Coomarasamy and Walzak, 1995; Xie et al., 2012). Some laboratory and field research results suggested that SSA was sensitive to the moisture damage (Chen et al., 2020; Chen et al., 2016a; Coomarasamy and Walzak, 1995), especially when the free-thaw effect were considered (Chen et al., 2020; Chen et al., 2016a).

The homogeneity of the properties of SSA is relatively poor due to the complex compositions and structures of steel slag, which is one of the possible reasons for the inconsistent research findings on the moisture stability of asphalt mixture with SSA. Coomarasamy and Walzak found that the debonding of the interface between SSA and asphalt mastic in asphalt pavement happened randomly, and the formation of calcium carbonate ($CaCO_3$)-rich deposits at the surface of some SSA particles in moist condition caused cracks (Coomarasamy and Walzak, 1995). It was inferred that the compositions of different SSA particles could be different. Some SSA particles have free lime (*f*-CaO) at the surface, which is the main cause for the $CaCO_3$-rich deposits, because *f*-CaO can be transformed into $CaCO_3$ by reacting with water and carbon dioxide ($CO_2$) in moist condition. It is essentially a carbonation reaction, which causes the expansion problem.

In order to eliminate the negative effect of *f*-CaO on the volume stability of steel slag, the weathering treatment method by placing steel slag in natural environment has been widely used. The original purpose is to make *f*-CaO fully react with water and $CO_2$ in advance. Chen et al. found that the silicate minerals in steel slag can also participate in the carbonation reaction (Chen et al., 2014c). The whole reaction process is illustrated in Fig. 1(a). Hence, for some SSA particles with rich silicate minerals, many $CaCO_3$ crystal products can be generated. They are adhered to the surface of SSA due to the gelling activity of silicate minerals, which makes the appearance of some SSA particles change from grey-black to grey-white (see Fig. 1(b)). Chen et al. found that these SSA particles with grey-white $CaCO_3$ product layer is very sensitive to the freeze-thaw damage when used in asphalt mixture. As shown in Fig. 1(c), moisture first damages the bonding interface between asphalt mastic and SSA. Then, moisture infiltrates into the product layer. The frost heave effect of moisture further causes the fracture of the $CaCO_3$ product layer, which accelerates the damage of moisture to the bonding interface. Hence, there is risk to use SSA in asphalt mixtures even after they have gone through weathering treatment.

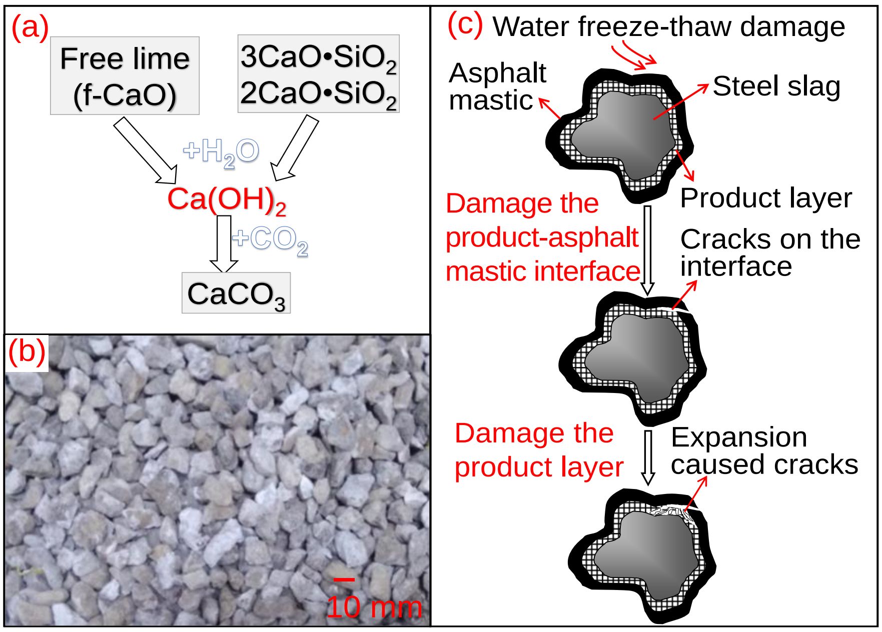


**Fig. 1** (a) Whole carbonation reaction of steel slag during weathering treatment; (b) appearance of SSA particles after weathering treatment; (c) freeze-thaw failure process of asphalt mixture with SSA (Chen et al., 2020; Chen et al., 2014c)

Considering the potential limitation of utilizing SSA in asphalt mixture, using steel slag powder (SSP) to replace mineral filler in asphalt mixture has been proposed. Although the dosage of filler in asphalt mixture is often less than 10%, it would still be a promising way to reuse steel slag efficiently because of the high demand of asphalt pavement construction and maintenance. So far, very few studies have been conducted on this topic. Li et al. investigated the effects of SSP on the rheological properties of asphalt mastic and the low-temperature performance of asphalt mixture (Li et al., 2017a; Li et al., 2017b). The complex compositions of steel slag, such as metallic iron and some solid solution phases, make steel slag very difficult to be grinded into SSP. Usually, grinding operation will be terminated when obtaining enough powder for experiment purposes. There are still lots of aggregate particles left without being fully grinded. Therefore, SSP prepared in the laboratory by partially grinding some aggregate particles cannot represent the average level of steel slag.

To address the concern of the poor homogeneity of the properties of SSA and SSP prepared in the laboratory, this study aims to develop a new SSP preparation method by fully grinding large volume of SSA with an industrialized production line. The feasibility of innovatively using industrially produced SSP in asphalt mixture to replace mineral filler was fully investigated. The following two research tasks were conducted as shown in Fig. 2:

(1) The chemical compositions and micro-morphologies of four SSPs were investigated to determine the homogeneity of the properties of SSPs and the advantages of using SSPs as asphalt fillers.

(2) Asphalt mixtures with different SSPs were designed by the Superpave method, and their main engineering performances, including moisture stability, high-temperature deformation resistance and low-temperature crack resistance, were evaluated.

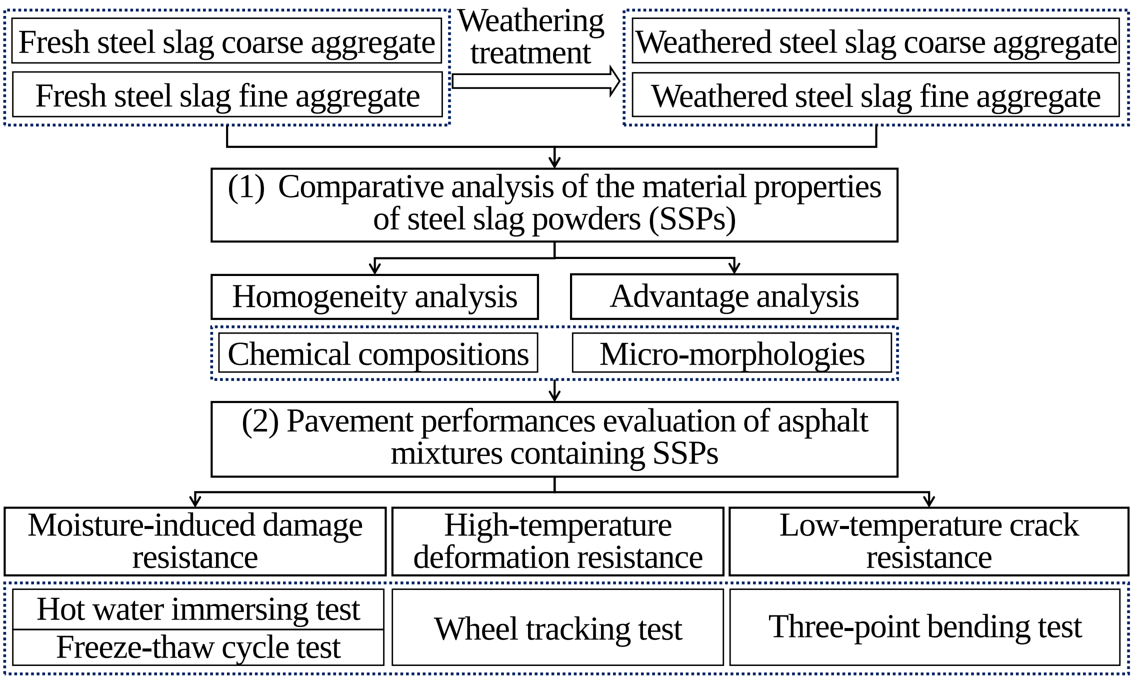


**Fig. 2** Flowchart of the research plan

## 2. Materials and methods

### *2.1. Raw materials*

In this research, five fillers, including four SSPs and one common limestone powder (LP), were used. SSPs were obtained by grinding a large volume of steel slag aggregates (more than 500 kg for each type of steel slag aggregate) with an industrialized production line. Raw steel slag was provided by the China Baowu Steel Group, which is basic oxygen furnace slag. Considering the weathering process during the storage of steel slag, four types of steel slag aggregates were used to produce SSPs, namely, fresh steel slag coarse aggregate (SSCA), weathered SSCA, fresh steel slag fine aggregate (SSFA) and weathered SSFA, and the corresponding SSPs were denoted as $SSP_{FC}$, $SSP_{WC}$, $SSP_{FF}$, $SSP_{WF}$, respectively. The weathering treatment duration was more than 6 months. Limestone powders and limestones for coarse and fine aggregates were both obtained from Yichang, Hubei Province, China. SBS modified asphalt produced by Hubei Guochuang Hi-Tech Material Co., Ltd. was used. The basic properties of the fillers, aggregates and SBS modified asphalt were tested according to the standard test methods (MOT, 2005), and results summarized in Tables 1-3.

**Table 1** Technical properties of fillers

| Parameter measured | | $SSP_{FC}$ | $SSP_{WC}$ | $SSP_{FF}$ | $SSP_{WF}$ | LP | Requirements according to Chinese specification (MOT, 2004) |
|---|---|---|---|---|---|---|---|
| Apparent density (g/cm$^3$) | | 3.468 | 3.477 | 3.322 | 3.326 | 2.707 | ≥ 2.5 |
| Percent passing (%) | 0.6 mm | 100 | 100 | 100 | 100 | 100 | 100 |
| | 0.15 mm | 92.8 | 92.5 | 92.1 | 92.3 | 92.7 | 90-100 |
| | 0.075 mm | 85.9 | 84.9 | 86.9 | 85.4 | 86.8 | 75-100 |

**Table 2** Technical properties of aggregates

| Parameter measured | Coarse aggregate | | Fine aggregate | Requirements according to Chinese specification (MOT, 2004) |
|---|---|---|---|---|
| | 16-9.5 mm | 9.5-4.75 mm | 4.75-0 mm | |
| Apparent specific gravity | 2.694 | 2.688 | 2.698 | ≥ 2.5 |
| Water absorption (%) | 0.5 | 0.4 | —— | ≤ 2.0 |
| Crush value (%) | 20.7 | —— | —— | ≤ 28 |
| Los Angeles abrasion (%) | 21.5 | 21.5 | —— | ≤ 30 |
| Flakiness and elongation (%) | 6.6 | 7.3 | —— | ≤ 18 |
| Fine aggregate angularity (s) | —— | —— | 52 | ≥ 30 |
| Sand equivalent (%) | —— | —— | 65 | ≥ 60 |

**Table 3** Technical properties of SBS modified asphalt

| Parameters | SBS modified asphalt | Requirements according to Chinese specification (MOT, 2004) |
|---|---|---|
| Penetration (25°C; 0.1mm) | 63 | 60-80 |
| Softening point (°C) | 76 | ≥ 55 |
| Ductility (5°C; cm) | 45 | ≥ 30 |
| Elasticity resume (25°C; %) | 71 | ≥ 65 |

### 2.2. Experimental methods

#### 2.2.1. Comparative analysis of the properties of SSPs

The chemical compositions and micro-morphologies of the SSPs were first characterized. The chemical compositions were analyzed by ethylene glycol-EDTA chemical titration and x-ray fluorescence (XRF). The former was to determine the content of *f*-CaO, and the later was for determining the average chemical compositions. Although *f*-CaO in steel slag is finally transformed into $CaCO_3$ after weathering treatment, some intermediate product, $Ca(OH)_2$, still exist. $Ca(OH)_2$ can also participate in the chemical titration reaction, as shown in the following equations:

$$CaO+C_2H_6O_2 \rightarrow (CH_2O)_2Ca+H_2O \tag{1}$$

$$Ca(OH)_2+C_2H_6O_2 \rightarrow (CH_2O)_2Ca+2H_2O \tag{2}$$

$$C_{10}H_{14}N_2Na_2O_8+(CH_2O)_2Ca \rightarrow C_{10}H_{14}N_2CaO_8+HOCH_2CH_2OH \tag{3}$$

Therefore, chemical titration gives the total content of $Ca^{2+}$ attributing to *f*-CaO and $Ca(OH)_2$. In this research, an auxiliary thermal gravimetric (TG) analysis device was used to determine the content of $Ca(OH)_2$ based on the mass change of each SSP in the decomposition temperature range. Finally, the content of *f*-CaO in SSP can be determined. The micro-morphologies of SSPs were observed by scanning electron micrograph (SEM).

The homogeneity of the properties of SSPs were analyzed based on the characterization results. SSA and LP were used as the control groups. In each characterization test, five replicates were prepared and tested. For each filler, the five powder samples were randomly picked out from the industrially produced SSPs and LP. For fresh SSCA and weathered SSCA, five particles with size of 19 mm were also randomly obtained from a large volume of SSA. For fresh SSFA and weathered SSFA, five samples with each composed of ten randomly selected particles with a size of 2.36 mm were used. In chemical titration and XRF analysis, they were grinded into powders in advance.

#### 2.2.2. Engineering performance evaluation of asphalt mixtures

In this study, the Superpave design method was applied to design the mixtures, and the standard test methods in accordance with the Chinese technical specifications were adopted to evaluate the engineering performances of the asphalt mixtures (MOT, 2011). High-temperature deformation resistance, low-temperature crack resistance and moisture damage resistance were determined by the wheel tracking test, three-point bending test, and retained Marshall stability (RMS) test and tensile strength ratio (TSR) test, respectively. In addition, the volume stability test of asphalt mixture was also included as a supplementary investigation.

*2.2.2.1. Design of asphalt mixture by the Superpave procedure*

Considering that only the filler types were different among the designed asphalt mixtures, each asphalt mixture was marked by the filler type, namely $SSP_{FC}$ mixture, $SSP_{WC}$ mixture, $SSP_{FF}$ mixture, $SSP_{WF}$ mixture and LP mixture. The proportions of the coarse aggregate, fine aggregate and filler in the mineral mixture were 46%, 50% and 4%, respectively. Although the particle size distributions of different fillers were not exactly same (see Table 1), they showed insignificant effect on the gradations of the mineral mixtures due to their low dosages. As a result, the gradations of these five mineral mixtures were almost the same. The used gradation is shown in Fig. 3. The optimum asphalt contents (OACs) of the asphalt mixtures were determined to be 4.9 %. It indicated that filler type has little effect on the OACs of the asphalt mixtures.

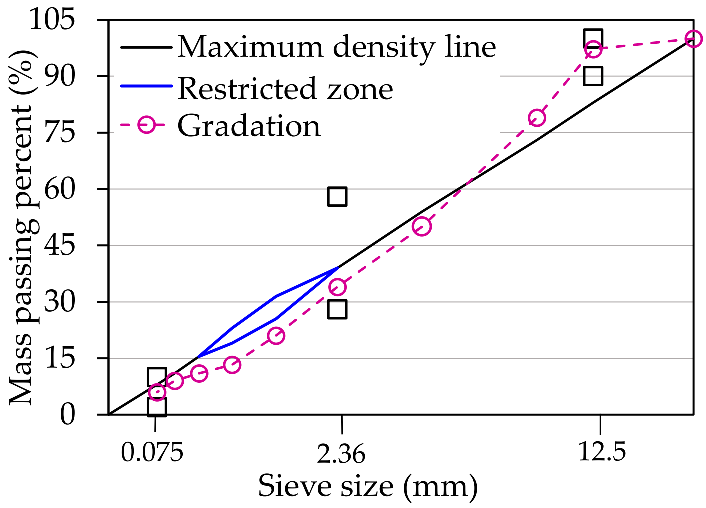


**Fig. 3** Aggregate gradation

*2.2.2.2. Moisture damage resistance evaluation*

Moisture stabilities of asphalt mixture are often determined by the RMS test and TSR test, which are conducted under hot water immersing damage condition and freeze-thaw cycle damage condition, respectively. The most noteworthy issue of reusing steel slag in asphalt mixture is the volume stability in hot and moist condition. Therefore, the volume stabilities of SSP asphalt mixtures under hot water immersing condition were also investigated in this research.

*Hot water immersing damage*. Specimens with a diameter of 100 mm and thickness of 63.5 mm and 4% air void content were used. The volume stability of the SSP asphalt mixture was checked by immersing specimens in a 60 $^{o}$C water bath and recording the volumes of the specimens every 24 h. The immersion operation lasted for 72 h. The volume expansion percentage of each specimen was calculated by the following equation:

$$p_{ve} = \frac{v_i - v_0}{v_0} \times 100\% \tag{4}$$

where $p_{ve}$ is the volume expansion percentage of specimen, %; $v_0$ is the original volume of the specimen, cm$^3$; and $v_i$ is the volume of the specimen after being immersed in hot water for $i$ h, cm$^3$.

For the RMS test, the same specimens for the volume stability tests were used, which were divided into four groups. One was the control group, and the other three were conditioned groups. Specimens in the conditioned groups were immersed in a water bath of 60 $^{o}$C for 24 h, 48 h and 72 h, respectively. The Marshall stabilities of the conditioned groups and control group were measured to determine the  RMS using the following equation:

$$RMS = \frac{MS_n}{MS_0} \times 100\% \tag{5}$$

where $MS_0$ is the average Marshall stability of the control group, kN; and $MS_n$ is the average Marshall stability of the conditioned group after being immersed in hot water for $n$ h, kN.

*Freeze-thaw cycle damage*. Cylindrical specimens with a diameter of 100 mm and thickness of 63.5 mm and air void content of 6% were prepared for the freeze-thaw cycle tests. The three conditioned groups were subjected to freeze-thaw damage for 1 cycle, 2 cycles and 3 cycles, respectively. One freeze-thaw cycle refers to freeze the specimens in a freezer at -18 $^{o}$C for 16 h , and then thaw them in the water bath at 60 $^{o}$C for 24 h. The indirect tensile strength (ITS) of each specimen was tested, and the following equation was used to measure the TSR:

$$TSR = \frac{ITS_h}{ITS_0} \times 100\% \tag{6}$$

where $ITS_0$ is the average ITS of the control group, MPa; and $ITS_h$ is the average ITS of the conditioned group after freeze-thaw damage for $h$ cycles, MPa.

*2.2.2.3. High-temperature deformation resistance*

Asphalt concrete slabs with 300 mm×300 mm×50 mm in size were used to evaluate the high-temperature performance of asphalt mixture. A simple wheel tracking device with a wheel load of 0.7 MPa was used. The wheel (50 mm width) moves back and forth along the center area of the specimens with a speed of 42 passes/min. Three test temperatures (50 $^{o}$C, 60 $^{o}$C and 70$^{o}$C) were considered. The high-temperature stability index of the asphalt mixture, named dynamic stability, was determined by the following equation:

$$DS = \frac{15 \times s}{d_{60} - d_{45}} \tag{7}$$

where $DS$ is the dynamic stability, pass/mm; $s$ is the wheel speed, pass/min; $d_{45}$ and $d_{60}$ are rutting depths of specimens corresponding to 45 min and 60 min, respectively, mm.

*2.2.2.4. Low-temperature crack resistance*

Low-temperature crack resistance of asphalt mixture was evaluated by the three-point bending test. The dimension of the beam specimens was 250 mm×30 mm×35 mm. UTM-30 with automatic temperature control and data acquisition system was utilized to bend the beam specimens at a vertical loading rate of 50 mm/min. The test temperature was -10 $^{o}$C. The flexural strength and strain were calculated by the following equations:

$$\sigma(t) = \frac{3lf(t)}{2bh^2} \times 10^3 \tag{8}$$

$$\varepsilon(t) = \frac{6hd(t)}{l^2} \times 10^6 \tag{9}$$

where $\sigma(t)$ is the flexural strength of beam specimen, MPa; $f(t)$ is the value of force loaded on beam specimen, kN; $l$, $b$ and $h$ are the spanning length, width and height of beam specimen, respectively, mm; $\varepsilon(t)$ is the strain of beam specimen, με; and $d(t)$ is the vertical deflection of beam specimen, mm. $\sigma(t)$, $f(t)$, $\varepsilon(t)$, and $d(t)$ are the functions of testing time $t$.

The Chinese technical specification for highway asphalt pavements construction focuses on the strain value when determining the low-temperature performance of asphalt mixture (MOT, 2004). But flexural strength may also affect the low-temperature performance of asphalt pavement. For example, higher flexural strength gives asphalt pavement better resistance to traffic load damage. Therefore, besides strain value, fracture energy, which involves both flexural strength and strain, was also calculated in this study using the following equation:

$$fe = 10^{-3} \int_0^{\varepsilon_f} \sigma d\varepsilon \tag{10}$$

where $fe$ is fracture energy, kJ/m$^3$; and $\varepsilon_f$ is the failure strain when $\sigma$ reaches the maximum value, με.

## 3. Results and discussions

*3.1. Properties of SSPs*

*3.1.1. Homogeneity analysis*

The contents of *f*-CaO in SSA particles and SSPs determined by the chemical titration method are shown in Fig. 4. It can be seen that, for aggregate particles, either SSCA or SSFA, the contents of *f*-CaO presented significant fluctuations. The error bars showed a standard deviation of 1.4%, 2.8%, 1.6% and 1.3% for randomly selected fresh SSCA, weathered SSCA, fresh SSFA and weathered SSFA particles, respectively. The average contents of *f*-CaO in the tested particles also displayed a strange trend: compared with the fresh SSCA and SSFA particles, weathered aggregate particles showed higher average contents of *f*-CaO, which contradicts to the expectation. Theoretically, the contents of *f*-CaO in weathered SSA particles should be lower. The compositions of steel slag are very complex, and the nonuniform distribution behaviors of some compositions can further explain the strange results shown in Fig. 4.

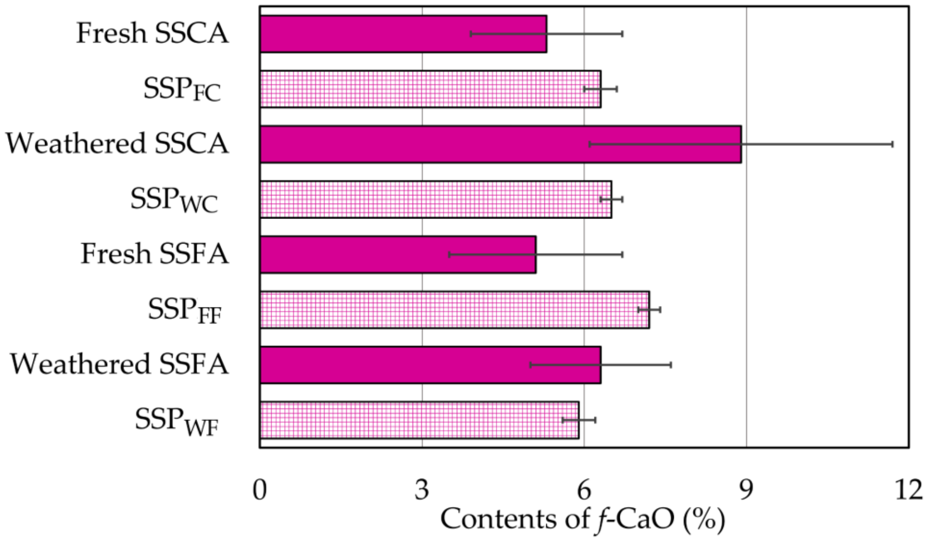


**Fig. 4** Contents of *f*-CaO in SSA particles and SSPs

The cross-sectional image of steel slag block indicated that some compositions of steel slag, such as metallic iron and *f*-CaO, were clustered rather than uniformly distributed (see picture a in Fig 5). The binary image shown in Fig. 5(b) more clearly illustrates their clustered distributions. Hence, zones of *f*-CaO enrichment would be included in some aggregate particles when preparing SSA by crushing steel slag blocks, and the contents of *f*-CaO in some aggregate particles would vary significantly, which lead to large-sized error bars of *f*-CaO content. Especially for the weathered SSCA, several zones of *f*-CaO enrichment have been observed when grinding two of the selected five particles.

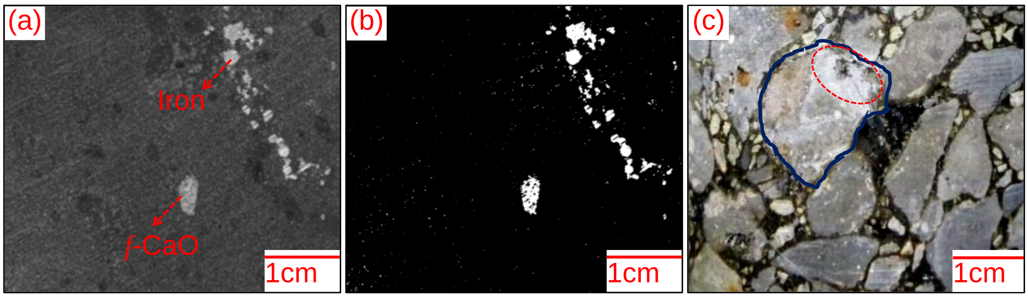


**Fig. 5** (a) Cross-sectional appearance of steel slag block; (b) binarization processed cross-sectional image; (c) localized expansion phenomenon of weathered SSCA based asphalt mixture

Although weathering treatment is a convenient way to reduce the expansion behavior caused by *f*-CaO, the carbonation reaction only occurs at the surface of SSA particles. So, the contribution of weathering treatment on the reduction of total *f*-CaO content is not significant. The content of *f*-CaO is highly dependent on the possible *f*-CaO enrichment region in the internal of SSA particles. Hence, the average contents of *f*-CaO in selected weathered SSA particles were not necessarily lower than those of selected fresh SSA particles considering the random distribution of *f*-CaO enrichment regions in different particles. As Fig. 4 shows, weathered SSCA and SSFA particles even possessed higher contents of *f*-CaO than fresh ones. The localized expansion cracks of weathered SSCA based asphalt mixture also supported this finding. Fig. 5(c) shows the broadside image of a cored asphalt mixture sample with weathered SSCA after hot water immersing damage. Localized expansion of weathered steel slag particle caused by *f*-CaO can be observed, indicating that the enrichment regions of *f*-CaO in the internal of steel slag particles remained even after weathering treatment.

The situation was quite different when SSPs were used. The four SSPs displayed very stable average contents of *f*-CaO. The error bars showed a standard deviation of 0.3%, 0.2%, 0.2% and 0.3% for $SSP_{FC}$, $SSP_{WC}$, $SSP_{FF}$ and $SSP_{WF}$, respectively. It indicated that grinding aggregate particles into SSPs was an effective way to overcome the significant variations of the contents of *f*-CaO in different SSA particles. Therefore, chemical titration results obtained based on SSPs were reliable to show the actual average level of *f*-CaO in steel slag. Particularly, there was no significant difference between the contents of *f*-CaO in $SSP_{FC}$ and $SSP_{WC}$, which also proved that carbonation reaction occurring at the surface of SSCA had minor effects on the average *f*-CaO content in steel slag. However, the contents of *f*-CaO for the SSPs prepared by grinding fresh SSFA and weathered SSFA were very different. As Fig. 4 shows, the *f*-CaO content of $SSP_{WF}$ was 18% lower than that of

$SSP_{FF}$. This is because the carbonation reaction efficiency of SSFA is higher than that of SSCA, contributed by the following two reasons: 1) the zones of *f*-CaO enrichment are more easily exposed to the surface of SSFA; and 2) the specific surface area of SSFA is larger.

The average chemical compositions of SSA particles and SSPs were determined by XRF. Some main chemical compositions are shown in Fig. 6. From Fig. 6a, it can be seen that, even for the same type of SSA, different particles presented significant difference in the contents of CaO, $SiO_2$ and $Fe_2O_3$, because of the complex compositions of aggregate particles. Fig. 6b shows that unlike the XRF results of SSA particles, the variations in the contents of the main chemical compositions of each SSP are very small as evidenced by the short error bars. Hence, XRF tests on SSPs are able to provide more reliable average chemical compositions of steel slag.

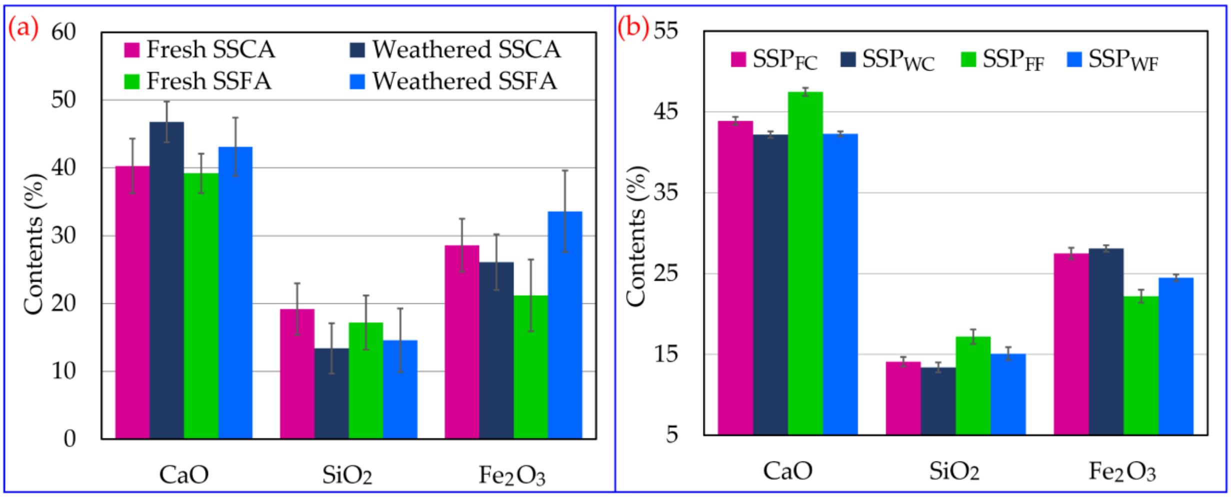


**Fig. 6** Main chemical compositions: (a) SSAs; (b) SSPs

From Fig 6(b), it can also be observed that the CaO contents of all SSPs were above 40%, while the corresponding *f*-CaO contents were less than 10% (see Fig. 4), which means that a large amount of CaO existed in other forms. Two forms of CaO have been reported. One was to form silicate minerals (dicalcium silicate and tricalcium silicate) with $SiO_2$, accordingly, the contents of $SiO_2$ were also substantial as shown in Fig. 6(b). For $SSP_{FC}$ and $SSP_{WC}$, the differences of CaO content and $SiO_2$ content were 1.7% and 0.7%, respectively. And which were 5.2% and 2.1%, respectively, for $SSP_{FF}$ and $SSP_{WF}$. It also supported the conclusion that the carbonation reaction of SSFA during the weathering process ran more thoroughly. More silicate minerals and *f*-CaO in SSFA participated in the carbonation reaction, and the relative contents of CaO and $SiO_2$ decreased because of absorbing $CO_2$ in the air. The other was to form a complex solid solution with some other oxides. The most important oxides in solid solution were these related to Fe element such as FeO and $Fe_2O_3$.

Besides ferrous and iron oxides, a great amount of Fe element existed in steel slag as metallic iron, as shown in Fig 5(a) and (b). They can be identified quickly because of some twills with the metallic luster. Fig 5(a) and (b) also showed that the metallic irons were clustered in steel slag blocks. Actually, many zones of metallic iron enrichment cannot be well-sorted out when crushing steel slag blocks although magnetic separation devices are configured. This is because some metallic iron is wrapped or non-magnetic. As a result, some SSA particles inevitably contain clustered metallic iron. And it is not easy to crush steel slag blocks containing metallic iron, therefore, coarse aggregate particles are more likely to occupy clustered metallic iron. It can explain why $SSP_{FC}$ and $SSP_{WC}$ presented higher densities than $SSP_{FF}$ and $SSP_{WF}$ (see Table 1). In fact, the contents of oxides given by XRF analysis are computed based on the concentrations of different elements. So the contents of $Fe_2O_3$ shown in Fig. 6 did not represent the actual amount of $Fe_2O_3$ in steel slag. To some extent, they showed the total contents of Fe element related compositions such as metallic iron and oxides. So, as shown in Fig 6(b), compared to $SSP_{FF}$ and $SSP_{WF}$, the contents of $Fe_2O_3$ in $SSP_{FC}$ and $SSP_{WC}$ given by XRF analysis were higher due to the contribution of more likely clustered metallic iron in coarse aggregate particles. As a result, the contents of other chemical compositions got lower relatively, such as lower content of CaO in $SSP_{FC}$ than that in $SSP_{FF}$.

The SEM test results indicated that the selected SSCA particles and SSFA particles all showed various micro-morphologies, and the main texture characteristics were almost the same. Therefore, only the micro-morphologies of SSCA particles before and after weathering treatment were analyzed in this research. As shown in Fig. 7(a), fresh SSCA particles mainly possessed three different surface structures, namely, dense structure, honeycomb structure and lamella structure. Some pores can be observed in the dense structure zone. The weathering process significantly modified the micro-morphologies of SSCA particles. It can be seen that, after weathering treatment, the dense structure zone was covered by carbonation reaction products of $CaCO_3$ (see Fig. 7(b)), indicating that the dense structure zone was rich in active minerals, which mainly included *f*-CaO and silicate minerals as shown in Fig. 1(a). And some small-sized products were embedded in the honeycomb structure zone (see Fig. 7 (c)). It suggested that the honeycomb structure zone was lack of active minerals. Many bar-shaped gypsum crystals were presented in the lamella structure zone (see Fig. 7(d)). They were quite different from $CaCO_3$ products. Therefore, except for carbonation reaction, some other reactions also occurred during weathering process although it was not the main reaction type. The various micro-morphologies of fresh and weathered SSCA particles also support the conclusion that the compositions and structures of SSA particles are complex and changeable.

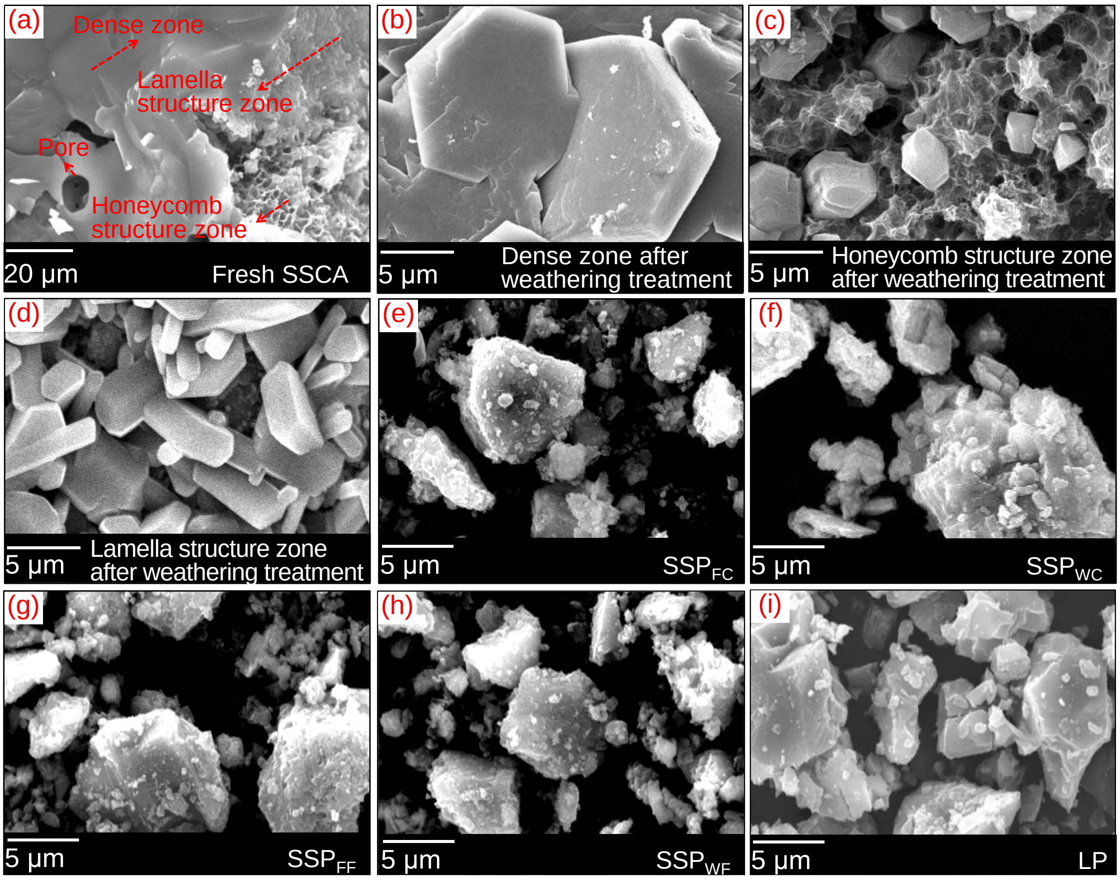


**Fig. 7** The micro-morphologies of SSCA and SSPs: (a) Fresh SSCA; (b) dense zone in Fresh SSCA after weathering treatment; (c) honeycomb structure zone in Fresh SSCA after weathering treatment; (d) lamella structure zone in fresh SSCA after weathering treatment; (e) SSP$_{FC}$; (f) SSP$_{WC}$; (g) SSP$_{FF}$; (h) SSP$_{WF}$; (i) LP

The homogeneity of the micro-morphologies of SSPs was much better than that of SSA particles. Fig. 7(e) to Fig. 7(h) displayed that the micro-morphologies of small-sized particles in four different SSPs were extremely similar. Their shapes were irregular, and the surface textures were very coarse. As a result, a conclusion similar to that in chemical composition analysis can be obtained. Compared to the changeable micro-morphologies of aggregate particles, grinding them into SSPs was also an effective way to homogenize the micro-morphologies of steel slag.

*3.1.2. Advantages of using SSPs as asphalt fillers*

The bonding behavior between aggregate and asphalt mastic directly influences the performances of asphalt mixture, especially the moisture damage resistance. Alkaline fillers such as Portland cement, hydrated lime was normally used to improve the engineering performances when constructing asphalt pavements in China. As a result, alkaline fillers are more than welcome. Mason has proposed an equation, $M=w(CaO)/[w(SiO_2)+w(P_2O_5)]$, to compute the alkalinity of steel slag (Mason, 1994). Steel slag is normally classified into three groups according to the value of alkalinity. They are low alkalinity slag ($M<1.8$), intermediate alkalinity slag ($1.8<M<2.5$) and high alkalinity slag ($M>2.5$) (Wang et al., 2011). The alkalinities of four SSPs in this research were shown in Fig.8, and they were determined based on the average chemical compositions of SSPs given by XRF. It can be seen that all alkalinities of the four SSPs were above 2.5, and it suggested that they were high alkalinity steel slags. It is well known that the common LP filler mainly contains $CaCO_3$ minerals. The carbonation of *f*-CaO and silicate minerals in SSPs also resulted in the generation of $CaCO_3$ minerals. It suggested that SSPs were more alkaline. Alkaline SSPs presented advantages when used as asphalt fillers. They improved the compatibility between filler particles and weak acid asphalt binder.

Specifically in Fig 8, although the carbonation reaction of some *f*-CaO and silicate minerals has absorbed some $CO_2$ during weathering treatment, it affected the alkalinity values of SSPs little. The differences of alkalinity values between $SSP_{FC}$ and $SSP_{WC}$, $SSP_{FF}$ and $SSP_{WF}$ were small. Actually, the content of $P_2O_5$ in steel slag is less than 1%, the alkalinity is mainly determined by the ratio of $w(CaO)$ to $w(SiO_2)$. Fig. 6(b) showed that the contents of CaO and $SiO_2$ in SSCA and SSFA both decreased after weathering treatment, especially that in SSFA. Therefore, low contents of *f*-CaO in $SSP_{WC}$ and $SSP_{WF}$ does not necessarily lead to low alkalinity values.

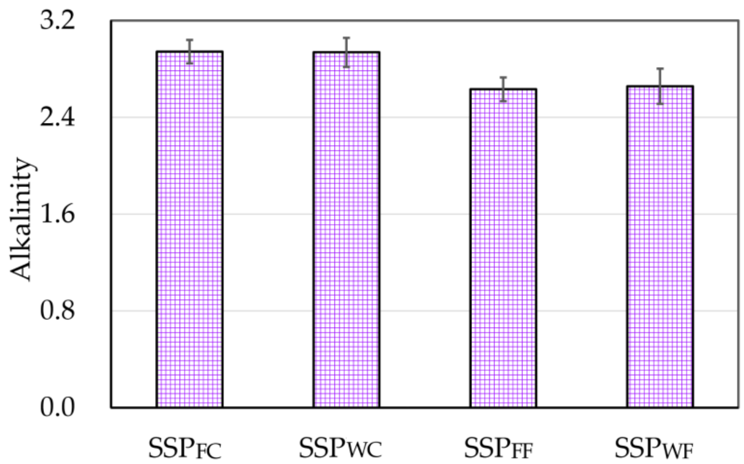


**Fig. 8** The computed alkalinity values of SSPs

While, Fig. 8 also showed that the alkalinity values of $SSP_{FF}$ and $SSP_{WF}$ were about 10% lower than that of $SSP_{FC}$ and $SSP_{WC}$. This may be due to the contribution of more silicate minerals in SSFA. As stated in the section of 3.1.1, compared to SSCA, SSFA was more likely to possess small amounts of clustered metallic iron. As a result, the contents of other minerals will be relatively higher, such as silicate minerals. Silicate minerals in steel slag mainly include dicalcium silicate($C_2S$) and tricalcium silicate ($C_3S$), and the ratios of $w$(CaO) to $w$($SiO_2$) are 1.87 and 2.8, respectively. The ratios of $w$(CaO) to $w$($SiO_2$) in $SSP_{FC}$ and $SSP_{WC}$ were around 3.0. Therefore, even the increased silicate minerals in SSFA were all $C_3S$, the ratios of $w$(CaO) to $w$($SiO_2$) in $SSP_{FF}$ and $SSP_{WF}$ would be still lower than that in $SSP_{FC}$ and $SSP_{WC}$.

The micro-morphologies of SSPs also gave an advantage in terms of using them as asphalt fillers. Pictures e to i in Fig.7 presented that the small particles in SSPs possessed rich convex and corrugated structures. While, the micro-surfaces of small particles in common LP were much smoother. The rich convex and corrugated micro-surfaces increased the specific surface area of SSPs and also raised the compatibility between SSPs and asphalt binder, which was beneficial for the stable bonding interaction between SSPs asphalt mastic and aggregate.

### *3.2. Performances of asphalt mixtures*

#### *3.2.1. Moisture damage resistance*

As Fig. 9 shows, the average volume expansion percentage of all asphalt mixtures were no more than 0.6% even after hot water damage for 72 h. The volume expansion percentage of asphalt mixture containing steel slag should be less than 1.5% according to the Chinese specification (MOT, 2004). Therefore, using SSPs as asphalt filler can give asphalt mixture satisfactory volume stability.

Even for the LP asphalt mixture, the volume expansion percent ranged from 0.45% to 0.56% with the increase of hot water damage time. Although the volume expansion percentage of asphalt mixtures containing different SSP showed some fluctuations when subjected to same amount of hot water immersion time, they were not obviously different from that of the LP asphalt mixture. The change interval for the volume expansion percent of SSPs asphalt mixtures was 0.39% to 0.6% when hot water damage time increased from 24 h to 72 h. Unlike the weathered SSCA asphalt mixture that presented a localized expansion phenomenon after hot water damage (see Fig. 5c), no cracks can be observed around the area of SSPs asphalt mastics. It indicated that the volume expansion of SSPs asphalt mixtures was not caused by the carbonization of *f*-CaO in SSPs. Instead, it was due to the natural thermal expansion effect of hot water to asphalt mixtures.

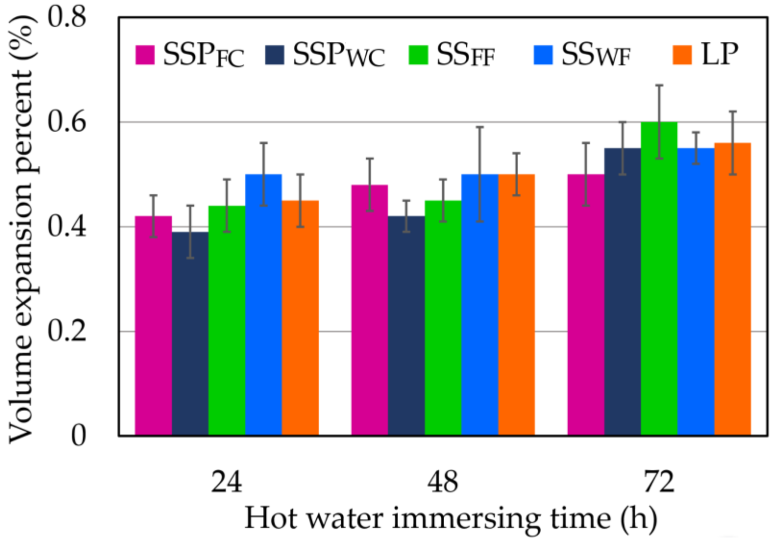


**Fig. 9** Volume stability test results of asphalt mixtures

The RMS results of asphalt mixtures are shown in Fig. 10, which indicated that the Marshall stabilities of asphalt mixtures were sensitive to the hot water damage. There was a significant drop in RMS value of each asphalt mixture when increasing the hot water immersing time. The RMS values of $SSP_{FC}$ mixture, $SSP_{WC}$ mixture, $SSP_{FF}$ mixture, $SSP_{WF}$ mixture and LP mixture decreased 11.9%, 11.4%, 10.1%, 10.6% and 12.6%, respectively, when hot water damage time reached 72 h. It indicated that SSPs played positive roles in improving the hot water damage resistance of asphalt mixtures. Fig. 10 also displayed that the weathering treatment has insignificant effects on the hot water damage resistance of asphalt mixtures. The differences of RMS values between $SSP_{FC}$ mixture and $SSP_{WC}$ mixture, $SSP_{FF}$ mixture and $SSP_{WF}$ mixture after hot water damage for the same time were very small. While, from the perspective of slag aggregate types, these two categories of SSPs prepared by grinding SSCA ($SSP_{FC}$ and $SSP_{WC}$) and SSFA ($SSP_{FF}$ and $SSP_{WF}$) respectively performed differently in maintaining the Marshall stabilities of asphalt mixtures. Although the RMS values of these four asphalt mixtures containing different SSP were very close after short-term hot water damage (24 h), the difference of the RMS values was gradually magnified with the increase of hot water damage time. Compared to $SSP_{FC}$ and $SSP_{WC}$, the asphalt mixtures containing $SSP_{FF}$ and $SSP_{WF}$, showed higher RMS values after longtime hot water damage. It suggested that $SSP_{FF}$ and $SSP_{WF}$ improved the durability of asphalt mixture in a high-temperature and moist environment. Therefore, the natural difference of material properties in SSCA and SSFA affected the hot water damage resistance of SSPs asphalt mixtures more obviously.

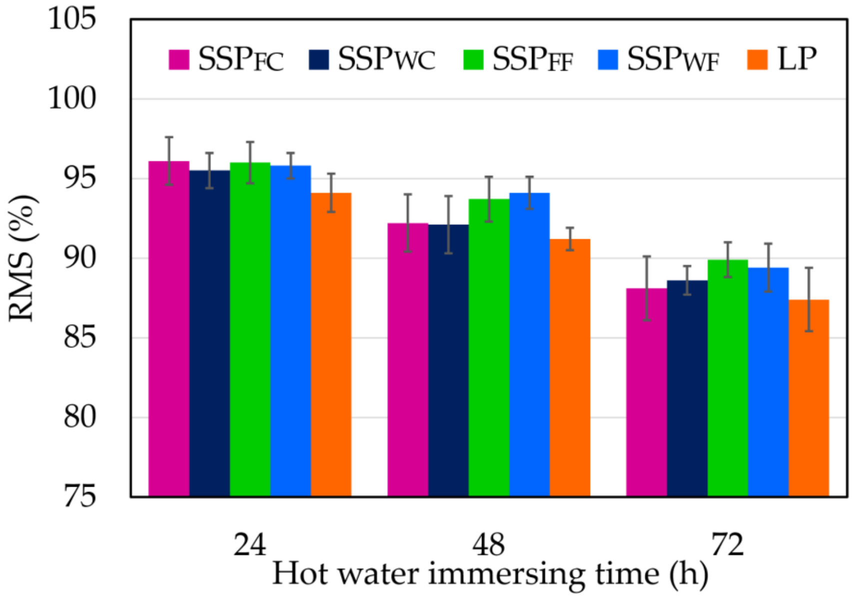


**Fig. 10** RMS results of asphalt mixtures

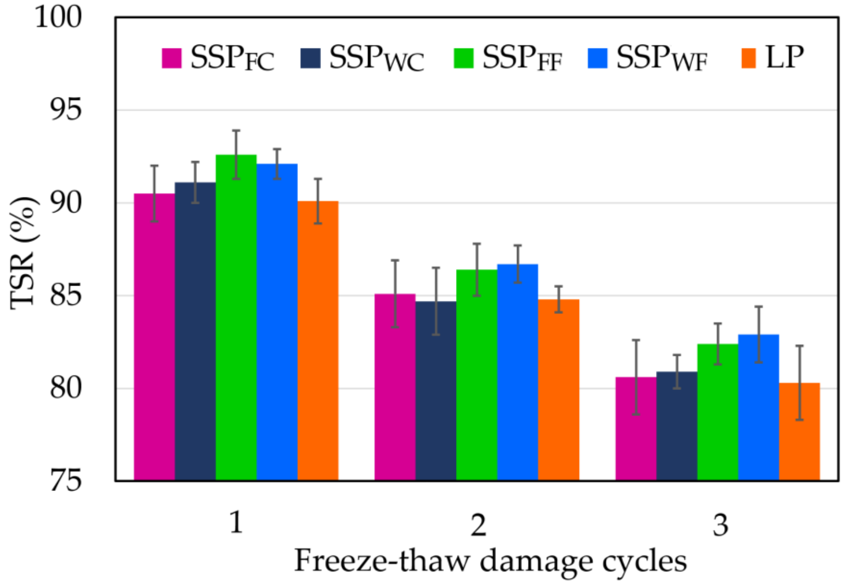


**Fig. 11** TSR results of asphalt mixtures

Fig. 11 presents the TSR results of SSPs asphalt mixtures, which showed similar trends as those of RMS. It can be seen that the indirect tensile strength of each asphalt mixture was also very sensitive to the freeze-thaw cycle damage. The TSR values of SSP$_{FC}$ mixture, SSP$_{WC}$ mixture, SSP$_{FF}$ mixture, SSP$_{WF}$ mixture and LP mixture decreased 19.4%, 19.1%, 17.6%, 17.1% and 19.7%, respectively, after suffering freeze-thaw damage for 3 cycles. In general, SSPs asphalt mixtures presented comparable or better freeze-thaw cycle damage resistance than LP asphalt mixture. Compared to LP, the advantages given by SSP$_{FC}$ and SSP$_{WC}$ were quite limited, while those provided by $SSP_{FF}$ and $SSP_{WF}$ were significant. Similar to the RMS results, TSR values of $SSP_{FC}$ mixture and $SSP_{WC}$ mixture, and of $SSP_{FF}$ mixture and $SSP_{WF}$ mixture after freeze-thaw conditioning were very close. Hence, the TSR results also supported that the natural difference of material properties in SSCA and SSFA influenced the freeze-thaw cycle damage resistance of SSPs asphalt mixtures more.

Although different types of SSP showed different abilities in maintaining the RMS and TSR values of asphalt mixtures, all SSPs always did better than LP, as shown in Fig. 10 and Fig. 11. It is widely agreed that the cohesion failure of the interior of asphalt mastic and the adhesion failure of the asphalt mastic and aggregate are the main damage forms of water to the asphalt mixture. For asphalt mastic, when using SSPs to replace common LP filler, the high alkalinity, rich convex and corrugated morphologies of SSPs improved the compatibility between filler particles and weak acid asphalt. On the one hand, the asphalt mastic itself was strengthened, and on the other hand, the adhesion performance of asphalt mastic and aggregate was also enhanced. As a result, SSPs played very positive roles in improving the moisture damage resistance of asphalt mixture.

*3.2.2. High-temperature deformation resistance*

The high-temperature deformation resistance of the Superpave asphalt mixture was evaluated by the wheel tracking test. The dynamic stabilities of asphalt mixtures computed based on wheel tracking test results are presented in Fig. 12. It is clear that SSPs strengthened the deformation resistance of asphalt mixtures at different test temperatures. At 50 °C, the dynamic stabilities of asphalt mixtures containing four different SSP were very close, which were approximately 10% higher that of LP asphalt mixture. But with the increase of test temperature, the contributions of four SSPs became different. $SSP_{FF}$ and $SSP_{WF}$ performed better in maintaining the deformation resistance of asphalt mixtures at 60 °C and 70 °C. It indicates that the SSPs manufactured by grinding SSFA played a positive role in improving the deformation resistance of asphalt mixture at higher temperatures, which may also be contributed by the natural difference of material properties in SSCA and SSFA.

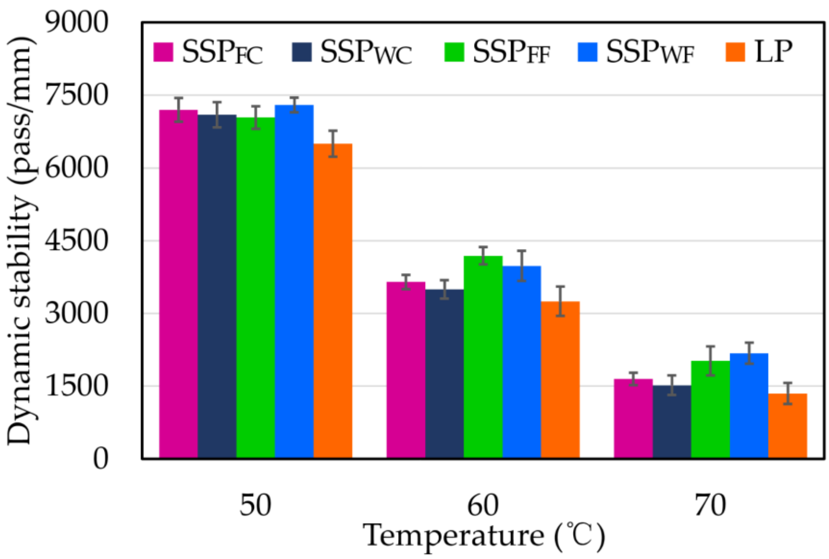


**Fig. 12** Dynamic stability results of asphalt mixtures

### *3.2.3. Low-temperature crack resistance*

The low-temperature crack resistance test results, i.e., low-temperature strain and fracture energy, of each asphalt mixture are presented in Fig. 13. It can be seen that the effects of SSPs on the low-temperature strain and fracture energy were inconsistent. The strain values of $SSP_{FC}$ mixture, $SSP_{WC}$ mixture, $SSP_{FF}$ mixture and $SSP_{WF}$ mixture were 6.2%, 8.8%, 4.9% and 2.9% lower than that of LP mixture, respectively, indicating that SSPs have hardened the asphalt mixture at low temperatures. But $SSP_{FF}$ and $SSP_{WF}$ performed better in maintaining the low-temperature strain than $SSP_{FC}$ and $SSP_{WC}$. The effect of SSPs on the fracture energy of asphalt mixtures was just the opposite. Fracture energy is determined based on both flexural strength and strain of asphalt mixture, as well as their correlation, so it is a more scientific index to determine the low-temperature performance of asphalt mixture. Fracture energy index has also been widely adopted in previous research (Wang et al., 2021; Zhang et al., 2019). Hence, the low-temperature bending test results indicated that SSPs improved the low-temperature crack resistance of asphalt mixtures in terms of fracture energy index, even though they have slightly lowered the strain values of asphalt mixtures.

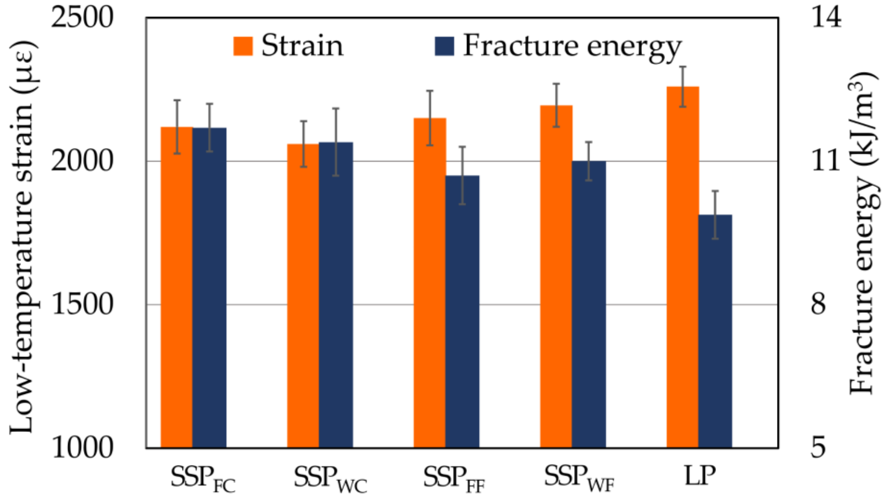


**Fig. 13** Low-temperature bending test results of asphalt mixtures

## 4. Conclusions

In this study, an innovative method of using SSP to replace mineral filler in asphalt mixture was proposed to address the concern of poor property homogeneity of steel slag aggregates. Four SSPs, including $SSP_{FC}$, $SSP_{WC}$, $SSP_{FF}$ and $SSP_{WF}$, were prepared by grinding large volume of fresh SSCA, weathered SSCA, fresh SSFA and weathered SSFA, respectively, using an industry production line, and investigated through a series of laboratory tests. Based on the results of the laboratory tests, the following major findings have been obtained:

(1) Unlike the nonhomogeneous chemical compositions and micro-morphologies of SSA particles, the chemical compositions and micro-morphologies of SSPs were much more uniform. In other words, grinding steel slag aggregates into SSPs can help homogenize the properties of steel slag.

(2) The high alkalinity, rich convex and corrugated morphologies of the four SSPs improved the compatibility between filler particles and weak acid asphalt binder, which was beneficial for the stable bonding interaction between SSPs asphalt mastic and aggregate.

(3) The four SSPs can significantly improve the moisture stability, high-temperature stability and low-temperature crack resistance of asphalt mixture. $SSP_{FF}$ and $SSP_{WF}$ performed better in improving the moisture stability and high-temperature stability, while $SSP_{FC}$ and $SSP_{WC}$ performed better in enhancing the low-temperature crack resistance.

## Acknowledgments

This work was financially supported by the Natural Science Foundation of China (Nos. 51808517 & 41731284 & 52008042), the Hong Kong Scholars Schedule (No. XJ2019041) and its matching fund from the Hong Kong Polytechnic University (G-YZ3J), the Hubei Chenguang Talented Youth Development Foundation, the Open Fund of Key Laboratory of Road Structure and Material of Ministry of Transport (Changsha University of Science & Technology) (No. kfj190302), the Open Fund of State Key Laboratory of Green Building Materials (No. 2021GBM03), the Open Fund of State Key Laboratory of Subtropical Building Science (No. 2022ZB17) and the National Students Innovation and Entrepreneurship Training Program (Nos. 201910491088 & 202010491075 & 202010491029 & S202110491095 & S202110491016).

## References

Ahmedzade, P., Sengoz, B., 2009. Evaluation of steel slag coarse aggregate in hot mix asphalt concrete. Journal of hazardous materials 165(1), 300-305.

Chang, X., Zhang, R., Xiao, Y., Chen, X., Zhang, X., Liu, G., 2020. Mapping of publications on asphalt pavement and bitumen materials: A bibliometric review. Construction and Building Materials 234, 117370.

Chen, Z., Gong, Z., Jiao, Y., Wang, Y., Shi, K., Wu, J., 2020. Moisture stability improvement of asphalt mixture considering the surface characteristics of steel slag coarse aggregate. Construction and Building Materials 251, 118987.

Chen, Z., Jiao, Y., Wu, S., Tu, F., 2018. Moisture-induced damage resistance of asphalt mixture entirely composed of gneiss and steel slag. Construction and Building Materials 177, 332-341.

Chen, Z., Wu, S., Li, F., Chen, J., Qin, Z., Pang, L., 2014a. Recycling of Flue Gas Desulfurization residues in gneiss based hot mix asphalt: Materials characterization and performances evaluation. Construction and Building Materials 73, 137-144.

Chen, Z., Wu, S., Wen, J., Zhao, M., Yi, M., Wan, J., 2015. Utilization of gneiss coarse aggregate and steel slag fine aggregate in asphalt mixture. Construction and Building Materials 93, 911-918.

Chen, Z., Wu, S., Xiao, Y., Zeng, W., Yi, M., Wan, J., 2016a. Effect of hydration and silicone resin on Basic Oxygen Furnace slag and its asphalt mixture. Journal of Cleaner Production 112, 392-400.

Chen, Z., Wu, S., Xiao, Y., Zhao, M., Xie, J., 2016b. Feasibility study of BOF slag containing honeycomb particles in asphalt mixture. Construction & Building Materials 124, 550-557.

Chen, Z., Xiao, Y., Pang, L., Zeng, W., Wu, S., 2014b. Experimental assessment of flue gas desulfurization residues and basic oxygen furnace slag on fatigue and moisture resistance of HMA. Fatigue & Fracture of Engineering Materials & Structures 37(11), 1242-1253.

Chen, Z., Xie, J., Xiao, Y., Chen, J., Wu, S., 2014c. Characteristics of bonding behavior between basic oxygen furnace slag and asphalt binder. Construction and Building Materials 64, 60-66.

Coomarasamy, A., Walzak, T., 1995. Effects of moisture on surface chemistry of steel slags and steel slag-asphalt paving mixes. Transportation research record(1492), 85-95.

Huang, Y., Bird, R.N., Heidrich, O., 2007. A review of the use of recycled solid waste materials in asphalt pavements. Resources, Conservation and Recycling 52(1), 58-73.

Leng, Z., Padhan, R.K., Sreeram, A., 2018a. Production of a sustainable paving material through chemical recycling of waste PET into crumb rubber modified asphalt. Journal of Cleaner Production 180, 682-688.

Leng, Z., Sreeram, A., Padhan, R.K., Tan, Z., 2018b. Value-added application of waste PET based additives in bituminous mixtures containing high percentage of reclaimed asphalt pavement (RAP). Journal of Cleaner Production 196, 615-625.

Li, C., Chen, Z., Wu, S., Li, B., Xie, J., Xiao, Y., 2017a. Effects of steel slag fillers on the rheological properties of asphalt mastic. Construction and Building Materials 145, 383-391.

Li, C., Xiao, Y., Chen, Z., Wu, S., 2017b. Crack resistance of asphalt mixture with steel slag powder. Emerging Materials Research 6(1), 214-218.

Mason, B., 1994. The constitution of some open-hearth slag. J Iron Steel Inst 11, 69-80.

MOT, 2004. Ministry of Transport of the People's Republic of China. Technical specifications for construction highway asphalt pavements. JTG F40, 2004 (In Chinese).

MOT, 2005. Ministry of Transport of the People's Republic of China. Test methods of aggregate for highway engineering. JTG E42, 2005 (In Chinese).

MOT, 2011. Ministry of Transport of the People's Republic of China. Standard test methods of bitumen and bituminous mixtures for highway engineering. JTG E20, 2011 (In Chinese).

MOT, 2021. The Annual Statistics of Traffic and Transportation Announced by Ministry of Transport of the People's Republic of China. Avialable on line: https://xxgk.mot.gov.cn/2020/jigou/zhghs/202105/t20210517_3593412.html. Cited on May 20, 2021.

Pasetto, M., Baliello, A., Giacomello, G., Pasquini, E., 2017. Sustainable solutions for road pavements: A multi-scale characterization of warm mix asphalts containing steel slags. Journal of Cleaner Production 166, 835-843.

Shen, D.-H., Wu, C.-M., Du, J.-C., 2009. Laboratory investigation of basic oxygen furnace slag for substitution of aggregate in porous asphalt mixture. Construction and Building Materials 23(1), 453-461.

Wang, F., Xiao, Y., Cui, P., Lin, J., Li, M., Chen, Z., 2020. Correlation of asphalt performance indicators and aging Degrees: A review. Construction and Building Materials 250, 118824.

Wang, Q., Yan, P., Han, S., 2011. The influence of steel slag on the hydration of cement during the hydration process of complex binder. Science China Technological Sciences 54(2), 388-394.

Wang, X.Y., Zhang, J.H., Li, K., Ding, Y., Geng, L.T., 2021. Cracking Analysis of Asphalt Mixture Using Semi-circle Bending Method. Iranian Journal of Science and Technology-Transactions of Civil Engineering 45(1), 269-279.

Wu, S., Xue, Y., Ye, Q., Chen, Y., 2007. Utilization of steel slag as aggregates for stone mastic asphalt (SMA) mixtures. Building and Environment 42(7), 2580-2585.

Xiao, F., Amirkhanian, S., Juang, C.H., 2007. Rutting resistance of rubberized asphalt concrete pavements containing reclaimed asphalt pavement mixtures. Journal of Materials in Civil Engineering 19(6), 475-483.

Xiao, F., Amirkhanian, S.N., Shen, J., Putman, B., 2009. Influences of crumb rubber size and type on reclaimed asphalt pavement (RAP) mixtures. Construction & Building Materials 23(2), 1028-1034.

Xie, J., Chen, J., Wu, S., Lin, J., Wei, W., 2013. Performance characteristics of asphalt mixture with basic oxygen furnace slag. Construction and Building Materials 38, 796-803.

Xie, J., Wu, S., Lin, J., Cai, J., Chen, Z., Wei, W., 2012. Recycling of basic oxygen furnace slag in asphalt mixture: Material characterization & moisture damage investigation. Construction and Building Materials 36, 467-474.

Xue, Y., Wu, S., Hou, H., Zha, J., 2006. Experimental investigation of basic oxygen furnace slag used as aggregate in asphalt mixture. Journal of Hazardous Materials 138(2), 261-268.

Zhang, J.P., Tan, H.Q., Pei, J.Z., Qu, T., Liu, W.L., 2019. Evaluating Crack Resistance of Asphalt Mixture Based on Essential Fracture Energy and Fracture Toughness. International Journal of Geomechanics 19(4).